Integrative Analysis of Nucleotide Metabolism–Related Genes Reveals a Diagnostic Signature and In Silico Functional Disruption in Hypertrophic Scarring

Qiyun Luo, BM[1]; Xia Yang, BM[2]; Jiangyong Shen, PhD[1]; Meirong Yan, MM[1]; Xiaoni Wang, MM[1]; Yujie Liang, BM[1]; Lifeng Guan, PhD[1,*]

Abstract

Hypertrophic scar (HTS) is a fibrotic skin disease characterized by excessive extracellular matrix accumulation and chronic inflammation. This study aimed to investigate cellular heterogeneity, immune alterations, and nucleotide metabolism-related biomarkers in HTS and to explore their potential mechanisms. Single-cell RNA sequencing data were analyzed using Seurat for cell clustering and annotation. Nucleotide metabolism activity was evaluated to identify key cell populations and candidate genes. Bulk transcriptomic datasets from the Gene Expression Omnibus (GEO) were used for differential expression analysis, and machine learning algorithms were applied to develop a diagnostic model. Sixteen cell clusters were identified, with macrophages showing prominent activation of nucleotide metabolism pathways and immune-related signaling. The optimal Enet + svmLinear model achieved strong predictive performance (area under the curve = 0.934), and Shapley Additive exPlanations analysis identified NCF1 and GPR34 as key predictive genes. These genes were also associated with immune cell infiltration. In vitro validation using THP-1-derived M2 macrophages showed that NCF1 and GPR34 promoted transforming growth factor-β1 secretion and enhanced fibroblast activation, while their knockdown reduced α-smooth muscle actin and collagen I expression. Collectively, this study reveals the important role of macrophage-associated nucleotide metabolism in HTS and identifies NCF1 and GPR34 as potential biomarkers and therapeutic targets.

Key words: hypertrophic scar; single-cell RNA sequencing; nucleotide metabolism; machine learning; immune microenvironment.

INTRODUCTION

Hypertrophic scar (HTS) is a common pathological outcome of wound healing following skin trauma, burns, or surgical procedures. It is characterized by aberrant fibroblast proliferation, excessive extracellular matrix (ECM) deposition, and persistent activation of the local inflammatory microenvironment.[1,2] Histologically, HTS presents with disorganized collagen fiber architecture and abnormal matrix remodeling. Clinically, it is frequently accompanied by pain, pruritus, and restricted mobility, thereby substantially impairing patients' appearance and quality of life.[3,4] Although therapeutic strategies such as laser therapy, local pharmacological interventions, and biologic agents have advanced in recent years, effective molecularly targeted approaches capable of precisely modulating HTS initiation and progression remain limited.[5] Therefore, elucidating the key molecular mechanisms underlying HTS formation is of considerable importance for identifying novel diagnostic biomarkers and therapeutic targets.

In recent years, metabolic reprogramming has been recognized as a central driver in the pathogenesis of various diseases. Beyond classical pathways such as glycolysis and lipid metabolism, nucleotide metabolism, an essential biological process that sustains cell proliferation, DNA replication

[1]*Department of Burn Plastic Surgery and Cosmetology, General Hospital of Ningxia Medical University, Yinchuan, Ningxia 750004, China;* [2]*Department of Gastroenterology, General Hospital of Ningxia Medical University, Yinchuan, Ningxia 750004, China*

Author contributions: Qiyun Luo (Conceptualization, Data curation, Formal analysis [lead], Writing—original draft, Writing—review & editing [equal]), Xia Yang (Formal analysis [supporting], Resources [equal], Writing—original draft, Writing—review & editing [supporting]), Jiangyong Shen (Data curation, Writing—original draft, Writing—review & editing [supporting]), Meirong Yan (Data curation, Writing—original draft, Writing—review & editing [supporting]), Xiaoni Wang (Writing—original draft, Writing—review & editing [supporting]), Yujie Liang (Writing—original draft [supporting]), and Lifeng Guan (Conceptualization [equal], Project administration [lead], Resources, Writing—original draft, Writing—review & editing [equal])

Funding: This work was supported by the Ningxia Medical University Institutional Research Project (No. XY2025017) and Ningxia Natural Science Foundation (No. 2026AAC031087).

Conflict of interest statement: The authors have no conflicts of interest to declare.

**Address correspondence to L.G. (email: 18009593639@163.com)*

© The Author(s) 2026. Published by Oxford University Press on behalf of the American Burn Association. This is an Open Access article distributed under the terms of the Creative Commons Attribution-NonCommercial License (https://creativecommons.org/licenses/by-nc/4.0/), which permits non-commercial re-use, distribution, and reproduction in any medium, provided the original work is properly cited. For commercial re-use, please contact reprints@oup.com for reprints and translation rights for reprints. All other permissions can be obtained through our RightsLink service via the Permissions link on the article page on our site—for further information please contact journals.permissions@oup.com.

https://doi.org/10.1093/jbcr/irag152

and repair, RNA transcription, and energy homeostasis, has garnered increasing attention in the context of abnormal tissue hyperplasia and fibrotic disorders.[6,7] Nucleotide metabolism not only supplies purine and pyrimidine substrates required for rapidly proliferating cells but also influences cell fate decisions by regulating cell cycle progression, DNA damage response pathways, and intracellular signal transduction.[8,9] Emerging evidence indicates that nucleotide metabolic pathways are frequently dysregulated in tumors, inflammatory diseases, and multiple organ fibrosis; however, their systematic role in HTS remains insufficiently characterized.[9–11]

From a pathological perspective, HTS formation is closely associated with sustained fibroblast activation, abnormal proliferation, and transdifferentiation into a myofibroblast phenotype. These processes exhibit a high dependency on nucleotide supply and metabolic homeostasis.[6,12–14] Accordingly, nucleotide metabolism–related genes are hypothesized to play critical regulatory roles in HTS development and may represent potential diagnostic or therapeutic targets. Nevertheless, comprehensive investigations of nucleotide metabolism in HTS are still lacking, and the specific genes exerting key regulatory functions have not yet been fully elucidated.

Therefore, the present study systematically identified nucleotide metabolism–related differentially expressed genes based on publicly available transcriptomic datasets. By integrating multiple machine learning algorithms, we constructed a diagnostic model for HTS and screened for core gene signatures with high discriminative performance. Furthermore, an in silico gene knockout strategy was employed to simulate functional impairment of the identified hub genes, enabling comprehensive evaluation of their impact on metabolic pathway activity, signaling networks, and immune-related processes. By focusing on nucleotide metabolic pathways, this study aims to provide novel theoretical insights and molecular tools for the early diagnosis and precision treatment of HTS.

METHODS

Processing and analysis of single-cell RNA sequencing (scRNA-seq) data

The scRNA-seq dataset GSE156326 was obtained from the Gene Expression Omnibus (GEO) database. The dataset included HTS tissues collected from 3 female patients undergoing elective scar excision surgery and normal skin tissues ($n = 3$) obtained from excess abdominal skin removed during elective abdominoplasty from healthy female donors aged 25-45 years.

Single-cell data processing and downstream analyses were performed using the SCP platform and the Seurat R package. Quality control was performed to remove low-quality cells, with cells retained based on the following criteria: $200 < \text{nFeature_RNA} < 4000$ and mitochondrial gene percentage $< 20\%$. After quality filtering, the data were normalized, and highly variable genes were identified for principal component analysis. The selected principal components were used for t-distributed stochastic neighbor embedding visualization and unsupervised clustering. Cell types were annotated using canonical marker genes from previous studies[15] and the CellMarker 2.0 database.

To evaluate nucleotide metabolic activity across distinct cellular subpopulations, nucleotide metabolism–related gene sets were systematically collected from the Molecular Signatures Database (MSigDB). The AddModuleScore function implemented in Seurat was used to calculate a nucleotide metabolism score for each cell. Differences in module scores among cell subsets were subsequently compared to identify key cell populations exhibiting significant nucleotide metabolic activation.

Acquisition of bulk transcriptomic data and differential expression analysis

Hypertrophic scar-related bulk transcriptomic datasets were retrieved from GEO, including GSE178411 and GSE44270. In the GSE178411 dataset, RNA expression profiles were obtained from human skin samples, including uninjured normal skin ($n = 26$) and HTS tissues ($n = 30$). This dataset was designated as the training cohort for model construction. Differential expression analysis between HTS and control samples in GSE178411 was performed using the limma package. Differentially expressed genes (DEGs) were identified based on the criteria of $P < .05$ and $|\log2\text{-fold change}| > 0.5$. The GSE44270 dataset was used as an external validation cohort. This dataset included normal skin and scar tissues collected from patients undergoing elective plastic surgery or scar excision procedures.

Identification of macrophage-specific marker genes in HTS

To identify genes associated with HTS macrophages, DEGs from bulk transcriptomic analysis were intersected with macrophage-specific marker genes identified from scRNA-seq analysis. The intersection analysis was performed using the VennDiagram package. The overlapping genes were retained for subsequent functional enrichment analysis and machine learning model construction. Functional enrichment analysis was performed using the clusterProfiler package in R. Gene Ontology and Kyoto Encyclopedia of Genes and Genomes (KEGG) pathway analyses were conducted to evaluate the biological functions and pathway characteristics of the overlapping genes. Terms with $P < .05$ were considered statistically significant.

Construction and evaluation of machine learning models

Machine learning models were constructed using the overlapping genes to develop an HTS prediction model. A total of 18 machine learning algorithms were systematically integrated, including LASSO, Stepglm, glmBoost, Elastic Net (Enet), Random Forest (RF), Support Vector Machine (svmRadial and svmLinear), k-Nearest Neighbor (kknn and knn), Partial Least Squares (pls and plsRglm), Linear Discriminant Analysis (LDA), Neural Network (nnet), Naïve Bayes (naive_bayes), Stepwise Quadratic Discriminant Analysis (stepQDA), Stepwise Linear Discriminant Analysis (stepLDA), Generalized Linear Model with Stepwise Regression (glmStepAIC), and LogitBoost. Different feature selection and classification algorithm combinations were integrated, generating 112 candidate models.

The GSE178411 dataset was used as the training cohort, and GSE44270 was used as an external validation cohort. The mean

area under the curve (AUC) across repeated validations was used to evaluate model performance, and the model with the highest AUC was selected as the optimal model. Receiver operating characteristic (ROC) curves were generated using the pROC package. Calibration curves and decision curve analysis were performed using the rms and rmda packages, respectively.

Shapley Additive exPlanations (SHAP) analysis

To enhance model interpretability, Shapley Additive exPlanations (SHAP) analysis was performed on the optimal model using the Fastshap and kernelshap packages. Shapley values were calculated for each feature gene to quantify their individual contributions to model predictions. This approach enabled the identification of the most influential core genes contributing to HTS diagnosis.

Immune cell infiltration analysis

In the GSE178411 dataset, the relative abundance of multiple immune cell subsets was estimated using the CIBERSORT algorithm implemented in R. Differences in immune cell infiltration levels between groups were assessed using the *t*-test. In addition, Pearson correlation analysis was performed to evaluate the associations between expression levels of model-derived signature genes and the infiltration levels of various immune cell types, thereby exploring potential links between core genes and the immune microenvironment.

Single-gene gene set enrichment analysis (GSEA)

Based on the GSE178411 dataset, single-gene gene set enrichment analysis (GSEA) was performed using GSEA software (version 4.4.0). Samples were stratified into high- and low-expression groups according to the expression level of each target core gene. The enrichment of biological pathways associated with differential gene expression was subsequently evaluated.

In silico single-cell gene knockout analysis

To validate the potential biological functions of core genes from a functional perturbation perspective, in silico gene knockout analysis was performed using the scTenifoldKnk package. Macrophage subpopulations were first extracted from the single-cell dataset, and their gene regulatory networks were constructed. Target genes were then computationally knocked out at the single-cell level to simulate transcriptomic alterations following gene loss. The effects of gene perturbation on downstream pathways and regulatory network topology were systematically evaluated, thereby inferring the regulatory roles of core genes in HTS-associated macrophage function.

THP-1 macrophage differentiation and cell transfection

Human monocytic THP-1 cells were purchased from Procell Life Science & Technology Co., Ltd. (Wuhan, China). THP-1 cells were cultured in RPMI-1640 medium supplemented with 10% fetal bovine serum (FBS) and 1% penicillin–streptomycin solution and maintained at 37°C in a humidified incubator containing 5% CO_2. Cells were passaged every 2-3 days to maintain logarithmic growth.

For macrophage differentiation, THP-1 cells were treated with phorbol 12-myristate 13-acetate (PMA; 320 nmol/L) for 18 h to induce differentiation into M0 macrophages. After removing residual PMA by washing with PBS, cells were cultured in fresh complete medium for recovery. M2 macrophage polarization was induced by further incubation with recombinant human interleukin-4 (IL-4; 20 ng/mL) and interleukin-13 (IL-13; 20 ng/mL) for 48 h.

To investigate the roles of NCF1 and GPR34 in M2 macrophage activation, THP-1 cells were infected with lentiviral vectors carrying sh-NCF1, sh-GPR34, or negative control shRNA (sh-NC) before PMA induction. Briefly, THP-1 cells were incubated with lentivirus in the presence of 4 μg/mL polybrene to enhance infection efficiency. After 48 h of infection, stable transfected cells were selected with 1.5 μg/mL puromycin for 5 days. Subsequently, the selected cells were subjected to PMA-induced differentiation and IL-4/IL-13-mediated M2 polarization as described above.

Establishment of co-culture system

For the macrophage–fibroblast co-culture system, human dermal fibroblasts (HDFs) were cultured in Dulbecco's modified Eagle's medium (DMEM) supplemented with 10% FBS at 37°C with 5% CO_2. A Transwell co-culture system was established using 6-well plates. Human dermal fibroblasts were seeded into the upper chambers at a density of 1×10^4 cells/cm^2, while THP-1-derived M2 macrophages were seeded into the lower chambers at the same density. After 48 h of co-culture, cells were collected for subsequent analyses.

Quantitative real-time PCR (qRT-PCR)

Total RNA was extracted from THP-1-derived macrophages using TRIzol reagent. The concentration and purity of extracted RNA were determined using a NanoDrop spectrophotometer. Equal amounts of RNA were reverse-transcribed into complementary DNA using a reverse transcription kit. Quantitative real-time polymerase chain reaction (PCR) was performed using SYBR Green PCR Master Mix on a real-time PCR detection system. The amplification conditions were set according to the manufacturer's protocol. The relative mRNA expression levels of CD206, NCF1, and GPR34 were calculated using the $2^{-\Delta\Delta Ct}$ method. All experiments were performed in triplicate.

Enzyme-linked immunosorbent assay (ELISA)

Cell supernatants were collected and centrifuged to remove cell debris. The concentration of transforming growth factor-β1 (TGF-β1) was measured using a commercially available enzyme-linked immunosorbent assay (ELISA) kit according to the manufacturer's instructions. Briefly, samples and standards were added to antibody-coated plates and incubated, followed by sequential incubation with detection antibodies and substrate solution. The absorbance was measured at 450 nm using a microplate reader.

Western blotting

Total proteins were extracted from cells using radioimmunoprecipitation assay lysis buffer supplemented with protease inhibitors. Protein concentrations were determined using

a bicinchoninic acid protein assay kit. Equal amounts of protein samples were separated by 10% SDS-polyacrylamide gel electrophoresis and subsequently transferred onto polyvinylidene difluoride membranes. After blocking with 5% skim milk for 1 h at room temperature, the membranes were incubated overnight at 4°C with primary antibodies against α-smooth muscle actin (α-SMA), collagen I (Col1), and glyceraldehyde-3-phosphate dehydrogenase. After washing, membranes were incubated with corresponding horseradish peroxidase-conjugated secondary antibodies for 1 h at room temperature. Protein signals were detected using an enhanced chemiluminescence detection system, and band intensities were quantified using ImageJ software. Glyceraldehyde-3-phosphate dehydrogenase was used as the internal loading control.

Statistical analysis

All statistical analyses were performed using R software (version 4.5.0) and GraphPad Prism software (version 10.1.3). Data from cell experiments are presented as mean ± SD from at least 3 independent experiments. For comparisons between 2 groups, an unpaired Student's *t*-test was applied. For comparisons among multiple groups, one-way analysis of variance followed by Tukey's post hoc test was used. Pearson correlation analysis was performed to evaluate linear associations between variables where applicable. A P-value $< .05$ was considered statistically significant.

RESULTS

Single-cell transcriptome analysis reveals cellular heterogeneity and functional characteristics of HTS

To systematically analyze the cellular composition and molecular characteristics of HTS, we analyzed scRNA-seq data to identify the major cell populations and their potential roles in scar formation. As shown in Figure 1A, low-quality cells were filtered out. Unsupervised clustering based on gene expression patterns identified 16 distinct cellular populations within HTS and normal skin tissues (Figure 1B and C). These cell clusters were annotated according to established cell-type marker genes and categorized into 7 major cell types: fibroblasts, smooth muscle cells/pericytes, endothelial cells, macrophages, T cells, keratinocytes, and melanocytes (Figure 1D). Representative marker genes of these cell types are shown in Figure 1E.

The distribution differences of the identified cell types in normal and HTS tissues are shown in Figure S1A. Compared with normal skin, HTS tissues exhibited altered cellular composition, particularly involving fibroblast and immune cell populations. To further characterize the molecular functional features of each cell type, DEGs between the specific cell type and other cells were identified, and the results were shown in Figure S1B–H. Based on these cell type-specific DEGs, KEGG pathway enrichment analysis revealed functional pathways associated with the specific cells (Figure 1F). For example, fibroblast-related DEGs were significantly enriched in pathways such as "cytoskeleton regulation," "ECM-receptor interaction," "integrin signaling pathway," and "Wnt signaling pathway"; immune-related cells such as macrophages and T cells were enriched in classic immune pathways such as phagosome, cytokine-receptor interaction, T cell receptor signaling, and Th1/Th2 differentiation (Figure 1G).

Abnormal activation of nucleotide metabolism pathway in HTS macrophages and its immuno-inflammatory molecular basis

To explore metabolic changes associated with cellular dysfunction in HTS, we evaluated nucleotide metabolism activity across different cell populations using the single-cell transcriptomic dataset. As shown in Figure 2A and B, nucleotide metabolism activity varied among different cell types, with macrophages showing the highest pathway activity compared with other cellular populations. Further analysis revealed that macrophages from HTS tissues exhibited significantly higher nucleotide metabolism scores than those from normal skin ($P < .001$; Figure 2C). These findings indicate that macrophages may undergo metabolic reprogramming during HTS formation, and enhanced nucleotide metabolism may contribute to their altered inflammatory phenotype.

To further identify genes associated with HTS macrophage activation, bulk transcriptomic data from the independent GSE178411 dataset were integrated with the single-cell analysis results. Differential expression analysis identified 5662 genes between HTS and normal skin samples (Figure 2D). By overlapping HTS-related differentially expressed genes with macrophage-specific genes identified from single-cell analysis, 228 candidate genes were obtained (Figure 2E). These overlapping genes were primarily enriched in macrophage activation, myeloid immune responses, inflammatory regulation, and responses to external stimuli. In addition, these genes were enriched in cellular structures involved in immune cell function, including the plasma membrane, phagosomes, and endocytic vesicles. The enriched molecular functions were mainly related to immune recognition and inflammatory signaling, such as cytokine interactions and chemokine receptor activity (Figure 2F). Kyoto Encyclopedia of Genes and Genomes pathway analysis further demonstrated that these candidate genes were involved in several inflammation-related pathways, including cytokine–receptor interaction, Toll-like receptor signaling, phagosome formation, and nuclear factor (NF)-κB signaling (Figure 2G).

Predictive performance of HTS based on multi-algorithm ensemble model and explainable analysis of key gene contributions

To identify potential molecular markers associated with HTS, we developed a machine learning-based prediction model using transcriptomic data. Multiple machine learning algorithms were evaluated, and the optimal model was established using an Enet (alpha = 0.3) combined with svmLinear algorithm. The model showed good predictive performance across different datasets, with an average AUC of 0.934 (Figure 3A). The AUC reached 0.99 in the training cohort (Figure 3B) and remained robust in the independent validation cohort GSE44270 (AUC = 0.878; Figure 3C). Decision curve analysis and calibration analysis further demonstrated the clinical applicability and reliability of the model (Figure 3D and E). To further identify the major molecular features contributing to HTS prediction, 7 candidate genes included in the model were analyzed, including CD207, CD53, CSF2RB, CYTH4,

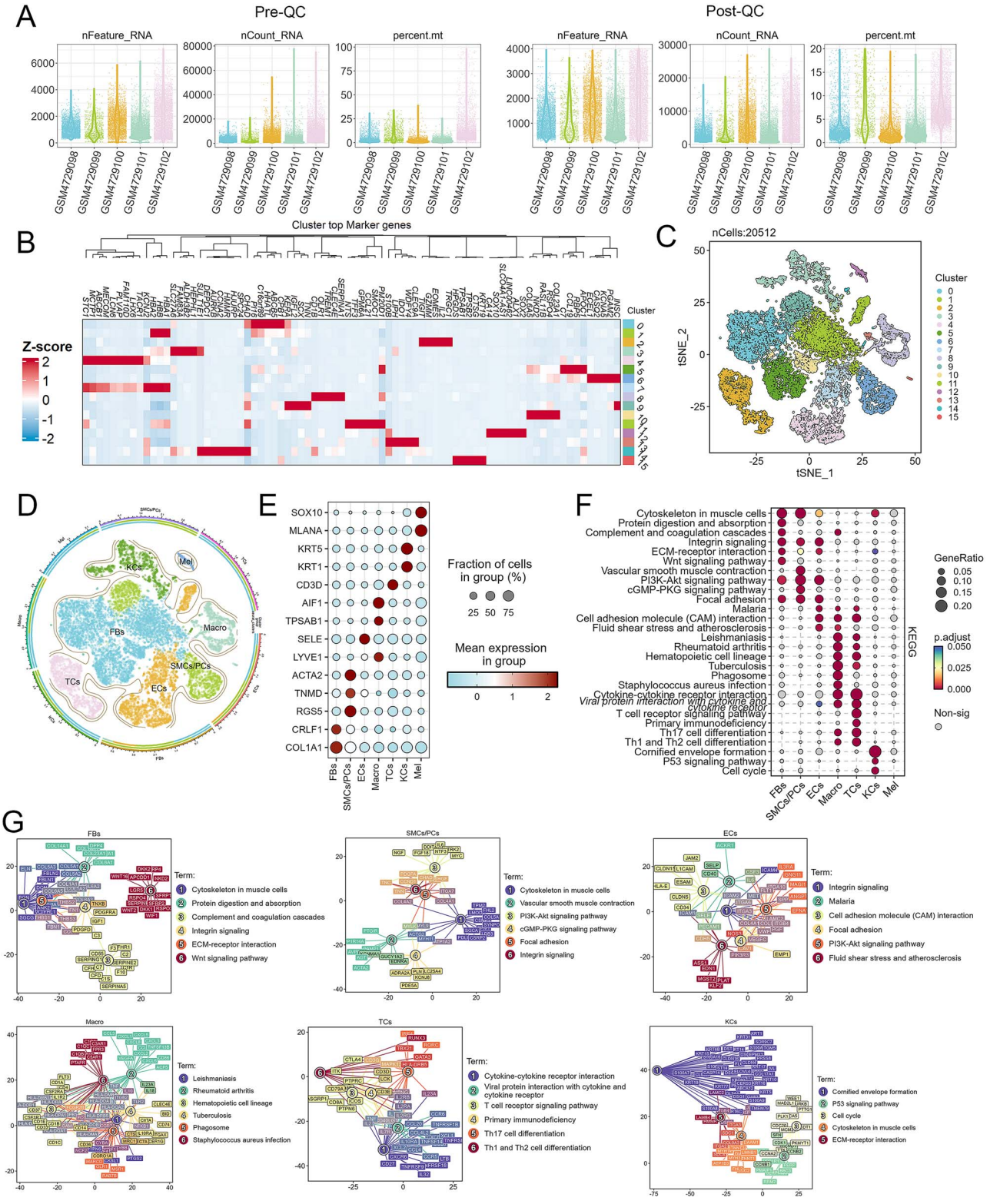


Figure 1. Cell-Type Annotation and Functional Characterization of Single-Cell Transcriptomic Profiles in Hypertrophic Scar (HTS) and Normal Skin Tissues. (A) Pre- and post-quality control filtering of single-cell transcriptomic data. (B) Heatmap of canonical marker gene expression used for cell-type annotation. (C) Unsupervised clustering identified 16 transcriptionally distinct cell clusters. (D) t-SNE visualization showing annotation of 16 cell clusters into 7 major cell types based on canonical marker gene expression. (E) Representative marker gene expression patterns for each annotated cell type. (F) KEGG pathway enrichment analysis of cell–type–specific differentially expressed genes. (G) Top enriched pathways for each cell type. Abbreviations: KEGG = Kyoto Encyclopedia of Genes and Genomes; t-SNE = t-distributed stochastic neighbor embedding.

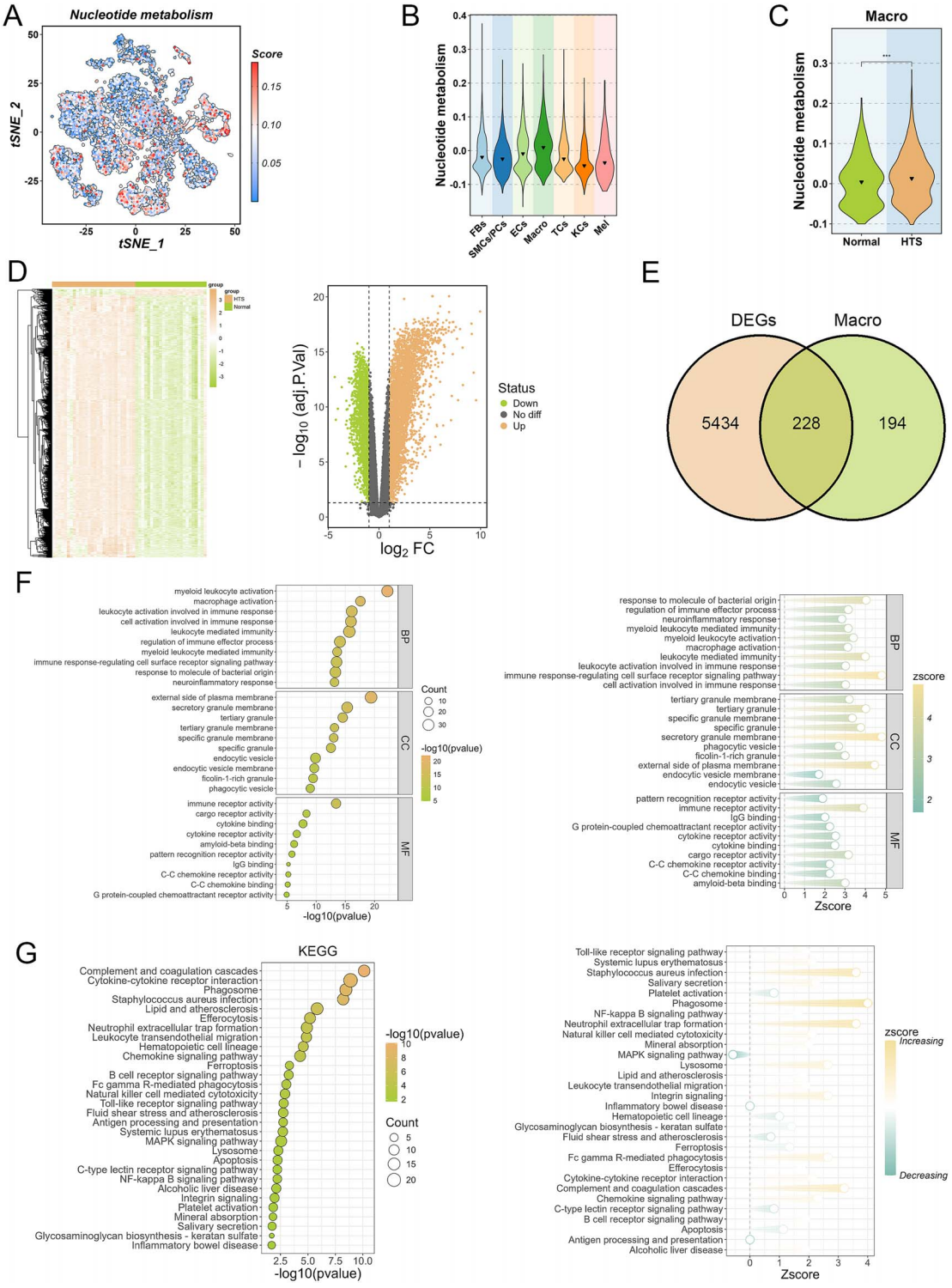


Figure 2. Aberrant Activation of the Nucleotide Metabolism Pathway in Hypertrophic Scar (HTS) Macrophages. (A) t-SNE visualization of single-cell transcriptomic data showing the distribution of nucleotide metabolism pathway scores across different cell populations. (B) Quantitative comparison of nucleotide metabolism pathway scores among 7 major cell types. (C) Comparison of nucleotide metabolism pathway activity between macrophages derived from HTS and normal tissues (***$P < .001$). (D) Differential gene expression analysis between HTS and normal samples using the GSE178411 dataset. (E) Venn diagram showing the intersection between DEGs from GSE178411 and macrophage-specific DEGs identified from single-cell analysis, yielding 228 overlapping genes. (F) Gene Ontology (GO) enrichment analysis of 228 overlapping genes, including biological process (BP), cellular component (CC), and molecular function (MF). (G) KEGG pathway enrichment analysis of the overlapping genes. Abbreviations: DEGs = differentially expressed genes; KEGG = Kyoto Encyclopedia of Genes and Genomes; t-SNE = t-distributed stochastic neighbor embedding.

GPR34, MRC1, and NCF1. Receiver operating characteristic analysis showed that these genes exhibited strong discriminative ability between HTS and normal samples in both training and validation cohorts (Figure 3F and G). Compared with normal skin, most model genes showed significantly increased expression in HTS tissues, suggesting their potential involvement in scar formation (Figure 3H).

Because machine learning models are often difficult to interpret biologically, we further applied SHAP analysis to determine the contribution of individual genes to model prediction. Among the 7 genes, NCF1 and GPR34 showed the highest contribution scores, followed by CYTH4, CD53, CD207, MRC1, and CSF2RB (Figure 4A). The SHAP analysis indicated that higher expression of NCF1, GPR34, and CYTH4 was associated with increased HTS prediction probability, suggesting that these genes may promote scar-associated biological changes. In contrast, CD53 and CD207 showed opposite trends, indicating potential protective or suppressive effects in HTS prediction (Figure 4B–I). MRC1 and CSF2RB contributed relatively less to the model prediction. The SHAP waterfall plot further illustrated how individual genes collectively influenced the final prediction result in a representative sample (Figure 4J). These findings identified NCF1 and GPR34 as the most influential candidate genes, providing potential targets for further functional investigation.

Biological characteristics of key model genes and their association with immune infiltration

Based on SHAP analysis, NCF1 and GPR34 were identified as the 2 most important genes contributing to HTS prediction. To explore their potential biological roles in scar formation, we further investigated their associated pathways and immune microenvironment characteristics. Gene set enrichment analysis results showed that GPR34 expression was associated with pathways involved in ECM remodeling, calcium signaling, and immune cell migration, including ECM–receptor interaction and leukocyte transendothelial migration (Figure 5A). These findings suggest that GPR34 may participate in HTS formation by regulating the microenvironment structure and immune cell recruitment. Similarly, samples with high NCF1 expression showed enrichment of pathways related to ECM regulation, immune activation, and cellular metabolism, including ECM-receptor interaction, leukocyte migration, and amino sugar and nucleotide sugar metabolism (Figure 5B). This suggests that NCF1 may regulate both immune cell function and metabolic adaptation during HTS development.

To further investigate the immune characteristics associated with HTS, immune cell infiltration analysis was performed. Compared with normal skin, HTS tissues showed significant alterations in immune cell composition, particularly involving macrophage populations (Figure 6A–C). Both M1 and M2 macrophages, as well as monocytes and activated dendritic cells, were increased in HTS tissues, whereas several resting immune cell populations showed reduced infiltration. Among these immune changes, the marked enrichment of M2 macrophages was particularly notable, supporting their potential role in promoting fibrosis and regulating the scar microenvironment. Changes in adaptive immune cell populations were also observed, including alterations in T follicular helper cells and regulatory T cells, suggesting that immune regulation is involved in maintaining the HTS microenvironment. Correlation analysis further demonstrated that NCF1 and GPR34 expression levels were positively associated with macrophage-related populations, especially M1/M2 macrophages and monocytes (Figure 6D). Their expression also showed associations with several other immune cell subsets, whereas weaker or negative correlations were observed with certain B-cell and CD4+ T-cell populations. Together, these findings indicate that NCF1 and GPR34 are closely linked to immune remodeling in HTS, particularly macrophage-associated inflammatory and fibrotic responses.

In silico gene knockout analysis of key model genes reveals their core role in immune and inflammatory regulation

To further explore the potential biological functions of NCF1 and GPR34 in HTS-associated immune regulation, we performed in silico knockout analysis based on transcriptomic data to investigate how changes in these genes may influence related molecular networks. The simulated loss of GPR34 or NCF1 expression resulted in widespread changes in gene expression profiles, indicating that both genes may be involved in regulating immune-related processes. In the GPR34 virtual knockout model, altered genes were mainly associated with macrophage function, complement activation, immune recognition, and inflammatory responses (Figure 7A). Several myeloid-related genes involved in immune homeostasis and macrophage activity, including C1QA, C1QB, C1QC, CD14, MS4A6A, and FOLR2, showed significant expression changes. Similarly, NCF1 virtual knockout resulted in transcriptional changes related to antigen presentation, immune activation, and myeloid cell function (Figure 7B). Genes involved in major histocompatibility complex (MHC)-mediated antigen presentation and immune cell activation, including human leukocyte antigen (HLA)-related genes, were significantly affected. In addition, genes associated with immune cell migration and myeloid differentiation also showed altered expression patterns, suggesting a potential role of NCF1 in maintaining immune cell activity and inflammatory responses. Functional enrichment analysis of the genes affected by virtual knockout further demonstrated that both GPR34 and NCF1 were associated with multiple immune-related pathways, including NF-κB signaling, complement activation, phagosome formation, antigen processing and presentation, and immune cell differentiation pathways (Figure 7C). These results suggest that NCF1 and GPR34 may serve as important regulators of macrophage-associated immune and inflammatory networks in HTS.

NCF1 and GPR34 promote M2 macrophage-mediated fibrotic activation

To investigate the roles of NCF1 and GPR34 in M2 macrophage-mediated fibrotic responses, THP-1 monocytes were first induced into M2 macrophages, followed by lentiviral knockdown of NCF1 or GPR34. As shown in Figure 8A, compared with M0 macrophages, M2 macrophages exhibited significantly increased mRNA expression of the M2 marker CD206, accompanied by elevated expression of NCF1 and GPR34 ($P < .001$). Knockdown of NCF1 or GPR34 markedly reduced their expression levels. Enzyme-linked immunosorbent assay

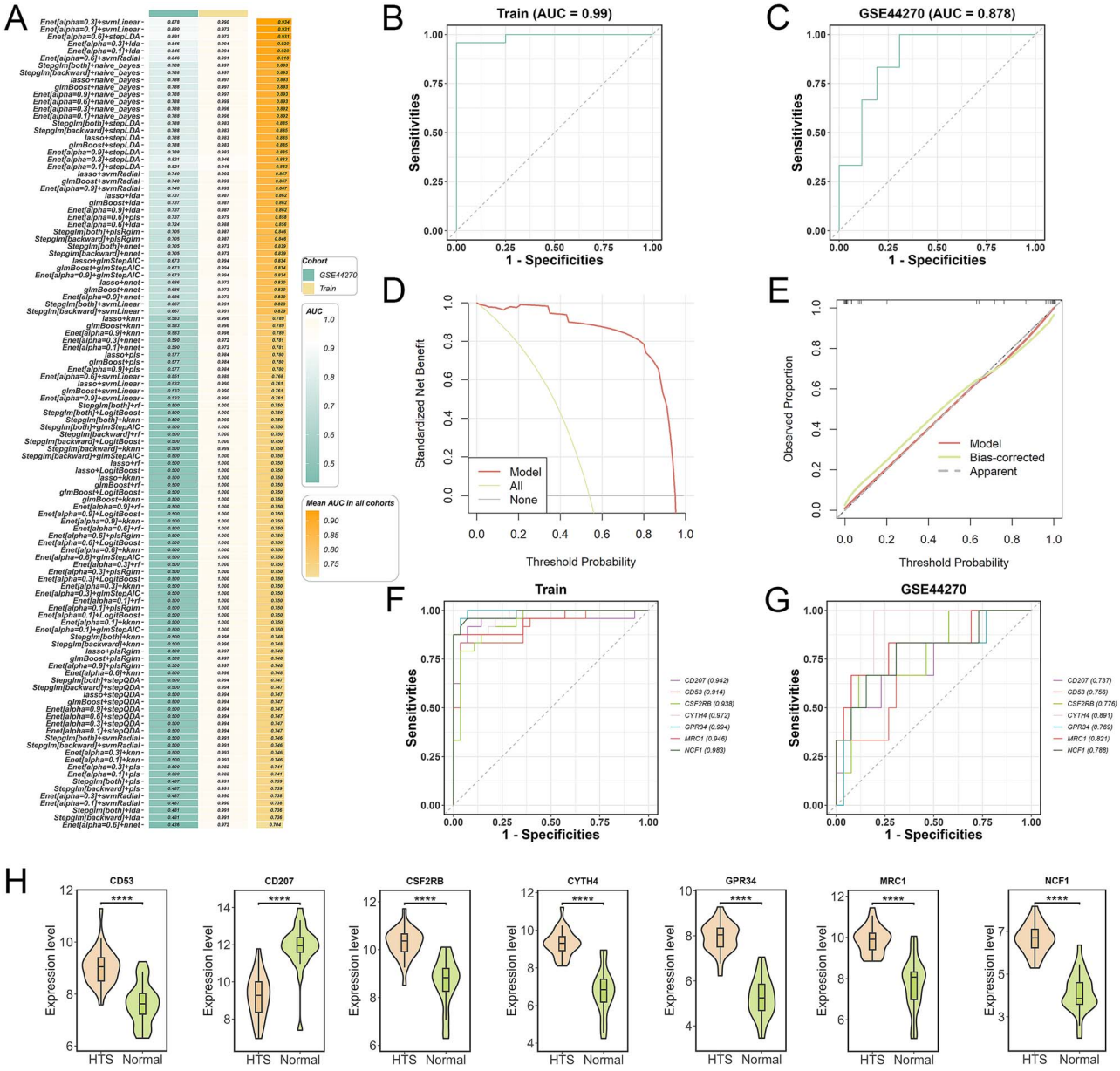


Figure 3. Construction and Validation of the Multi-Algorithm Ensemble Model for HTS Prediction. (A) Performance comparison of 18 machine learning algorithms and 112 model combinations. (B) ROC curve of the optimal model in the training set. (C) ROC curve in the independent validation cohort GSE44270. (D) Decision curve analysis (DCA) showing significant standardized net benefit across a wide range of threshold probabilities. (E) Calibration curve indicating high agreement between predicted probabilities and observed outcomes. (F–G) ROC curves of 7 model genes (CD207, CD53, CSF2RB, CYTH4, GPR34, MRC1, and NCF1) in the training and validation sets. (H) Differential expression analysis of model genes between normal and HTS tissues (****$P < .0001$). Abbreviations: HTS = hypertrophic scar; ROC = receiver operating characteristic.

analysis showed that M2 macrophages significantly increased the secretion of TGF-β1 compared with M0 macrophages ($P < .001$; Figure 8B). However, silencing NCF1 or GPR34 significantly reduced TGF-β1 production. To further evaluate the pro-fibrotic effects of M2 macrophages, THP-1-derived M2 macrophages were co-cultured with human dermal fibroblasts using a Transwell system. Western blotting analysis of HDFs after co-culture demonstrated that knockdown of NCF1 or GPR34 in M2 macrophages significantly attenuated the expression of fibrosis-associated markers α-SMA and collagen I (Col1) ($P < .001$; Figure 8C). Collectively, these findings suggest that NCF1 and GPR34 regulate M2 macrophage-mediated fibroblast activation and fibrotic responses.

DISCUSSION

This study employed scRNA-seq to comprehensively characterize the molecular landscape of HTS tissues, thereby elucidating cellular heterogeneity and immune functional alterations within the scar microenvironment. Although cell

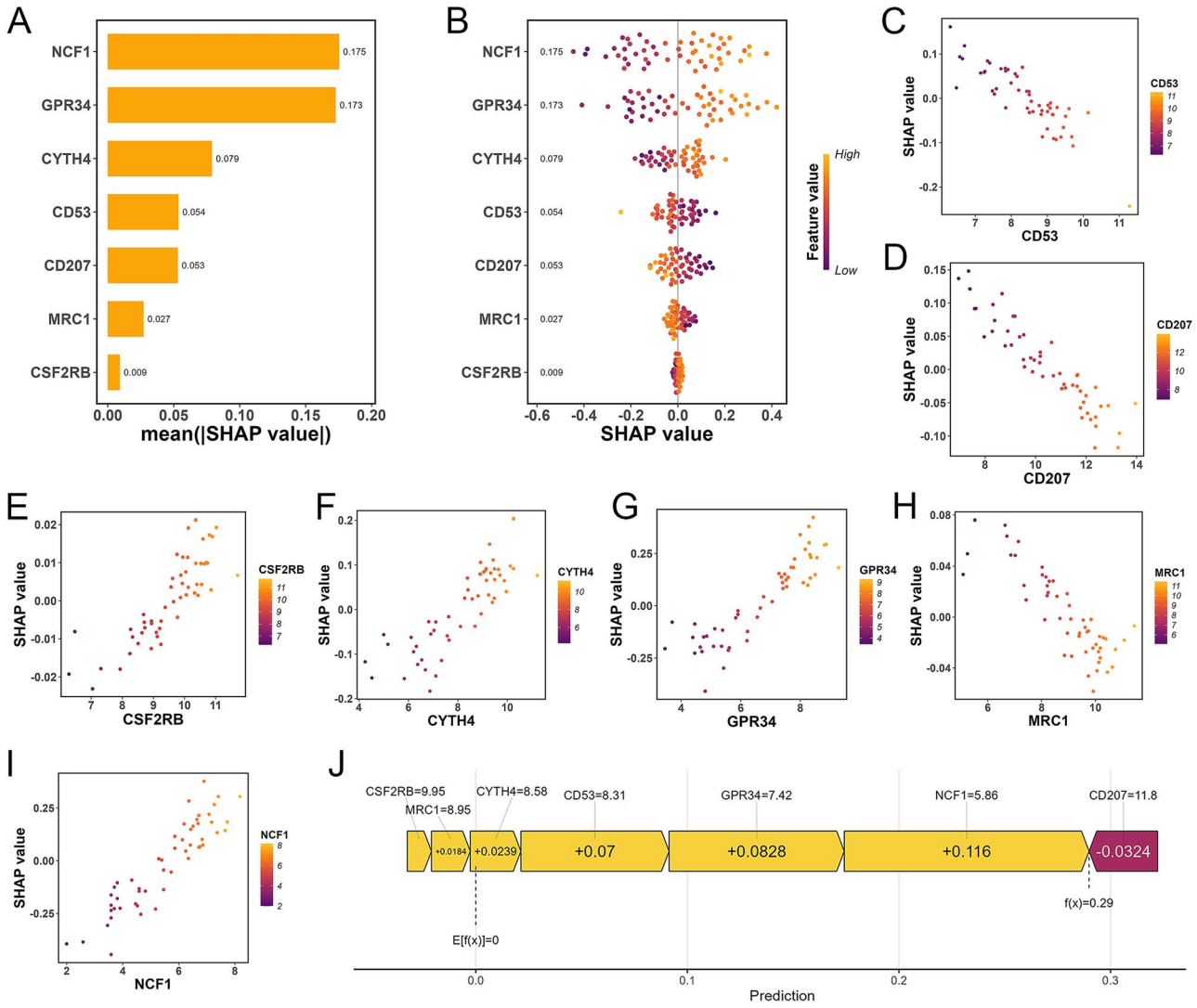


Figure 4. SHAP-Based Explainable Analysis of Key Gene Contributions in the HTS Prediction Model. (A) Feature importance ranking based on mean absolute SHAP values. (B) SHAP summary plot illustrating the direction and magnitude of each gene's contribution to HTS prediction across samples. (C–I) SHAP dependence plots for individual genes. (J) SHAP waterfall plot for a representative sample. Abbreviations: HTS = hypertrophic scar; SHAP = Shapley Additive exPlanations.

distributions largely overlapped across different samples, comparative analysis revealed marked differences in cellular composition between HTS and normal tissues, particularly in the proportions of fibroblasts and immune cell subsets. This pattern of "structural similarity with functional imbalance" suggests that HTS is not merely the consequence of aberrant proliferation of a single cell type, but rather a pathological process driven by multicellular dysregulation and intercellular crosstalk.

As the principal effector cells in HTS, fibroblasts exhibited a pronounced expansion and significantly elevated expression of ECM-related genes, including COL1A1 and COL1A2, further substantiating their dominant role in collagen deposition and matrix remodeling. Previous studies have established that persistently activated fibroblasts and their differentiation into myofibroblasts constitute a central mechanism underlying sustained scar hyperplasia.[1,2,16,17] Kyoto Encyclopedia of Genes and Genomes pathway enrichment analysis in the present study demonstrated that fibroblasts were significantly enriched in pathways related to cytoskeletal regulation and ECM–receptor interaction. These findings indicate that fibroblasts not only participate in matrix synthesis but may also enhance mechanosensing and mechanical responsiveness through integrin-mediated signaling and cytoskeletal remodeling. Mechanical stress has been recognized as a critical extrinsic driver of persistent scar formation,[18,19] and our single-cell transcriptomic data provide molecular-level evidence supporting this concept. Importantly, this study also revealed parallel alterations in fibroblast and immune cell populations at the single-cell level, suggesting that fibroblast abnormalities do not occur in isolation but are likely sustained by continuous stimulation from the immune microenvironment. Hypertrophic scar is fundamentally considered a chronic inflammatory disorder, in which the coupling between inflammation and fibrosis

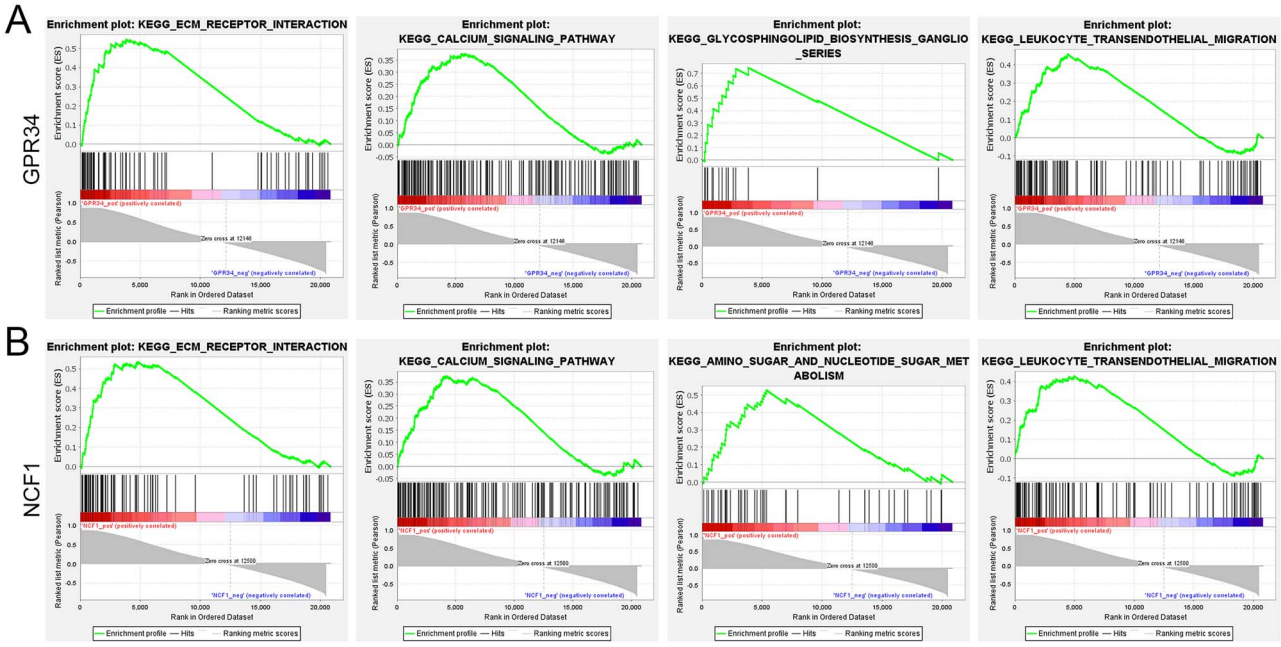


Figure 5. Gene Set Enrichment Analysis (GSEA) Enrichment Analysis of Core Model Genes GPR34 and NCF1 in HTS. (A) GSEA results for GPR34. (B) GSEA results for NCF1.

constitutes a key pathological basis for disease persistence.[20] During the early phase of wound healing, inflammation is essential for clearing necrotic tissue and initiating repair programs. However, when inflammatory signaling fails to resolve appropriately, the persistent inflammatory milieu continuously stimulates fibroblast activation and proliferation through the secretion of profibrotic mediators such as TGF-β, IL-6, and tumor necrosis factor (TNF)-α. Among these, the TGF-β/SMAD signaling axis is widely regarded as the central pathway in fibrogenesis, promoting the differentiation of fibroblasts into α-SMA–positive myofibroblasts and enhancing their contractile function and collagen synthesis capacity.[17,21] Interleukin-6 has been reported to modulate fibroblast proliferation and migration via the STAT3 signaling pathway,[22] while TNF-α may synergize with TGF-β signaling during the chronic phase to exacerbate matrix deposition.[23] Under prolonged exposure to such intertwined pro-inflammatory and profibrotic signals, fibroblasts progressively acquire a self-sustaining activation state, characterized by autocrine cytokine production and matrix-mediated feedback signaling. This ultimately leads to excessive collagen accumulation and progressive tissue stiffening, hallmark features of HTS formation.

In addition to fibroblasts, our results revealed significant alterations in both the proportion and transcriptional activity of macrophages and T cells. Macrophages were markedly increased in HTS tissues and exhibited a shift toward an M2-like phenotype. M2-polarized macrophages are known to secrete profibrotic mediators, including TGF-β1, PDGF, and CCL18, which directly promote fibroblast proliferation, collagen synthesis, and differentiation into myofibroblasts.[24–26] Moreover, macrophage-derived exosomes can transport miRNAs and various growth factors, thereby amplifying fibrotic signaling and strengthening intercellular communication.[27,28] T cells likewise play a pivotal regulatory role in the inflammation–fibrosis network. Interleukin-4 and IL-13 secreted by Th2 cells facilitate macrophage polarization toward the M2 phenotype and directly enhance collagen production in fibroblasts. In contrast, IL-17 produced by Th17 cells induces fibroblasts to secrete IL-6 and multiple chemokines, thereby establishing an inflammatory amplification loop.[29,30] Tregs are traditionally considered anti-inflammatory; however, in chronic fibrotic environments, their immunosuppressive function may paradoxically contribute to the persistence of inflammatory signaling, indirectly promoting fibrogenesis.[29,31] In our study, macrophage subsets in HTS tissues exhibited gene expression profiles enriched in cytokine production and chemokine signaling pathways, while transcriptional alterations in T cells paralleled fibroblast expansion. Collectively, these findings further support a pathological model in which sustained inflammation drives progressive fibrosis. Through the secretion of profibrotic cytokines, regulation of phenotypic polarization, and establishment of positive feedback signaling circuits, macrophages, and T cells cooperatively maintain aberrant fibroblast activation, thereby promoting persistent scar hyperplasia and matrix remodeling in HTS.

At the metabolic level, this study specifically focused on the nucleotide metabolic characteristics of macrophages and identified significantly enhanced nucleotide metabolic activity in HTS-derived macrophages. Previous studies have demonstrated that de novo purine and pyrimidine synthesis pathways are selectively activated in inflammatory macrophages, increasing intracellular GTP and ATP levels. This metabolic reprogramming enhances NF-κB-dependent transcriptional activity and inflammatory cytokine production while supporting rapid transcription and translation of inflammation-related mRNAs.[32–34] Furthermore, extracellular ATP and purinergic receptor signaling have been implicated in inflammatory ampli-

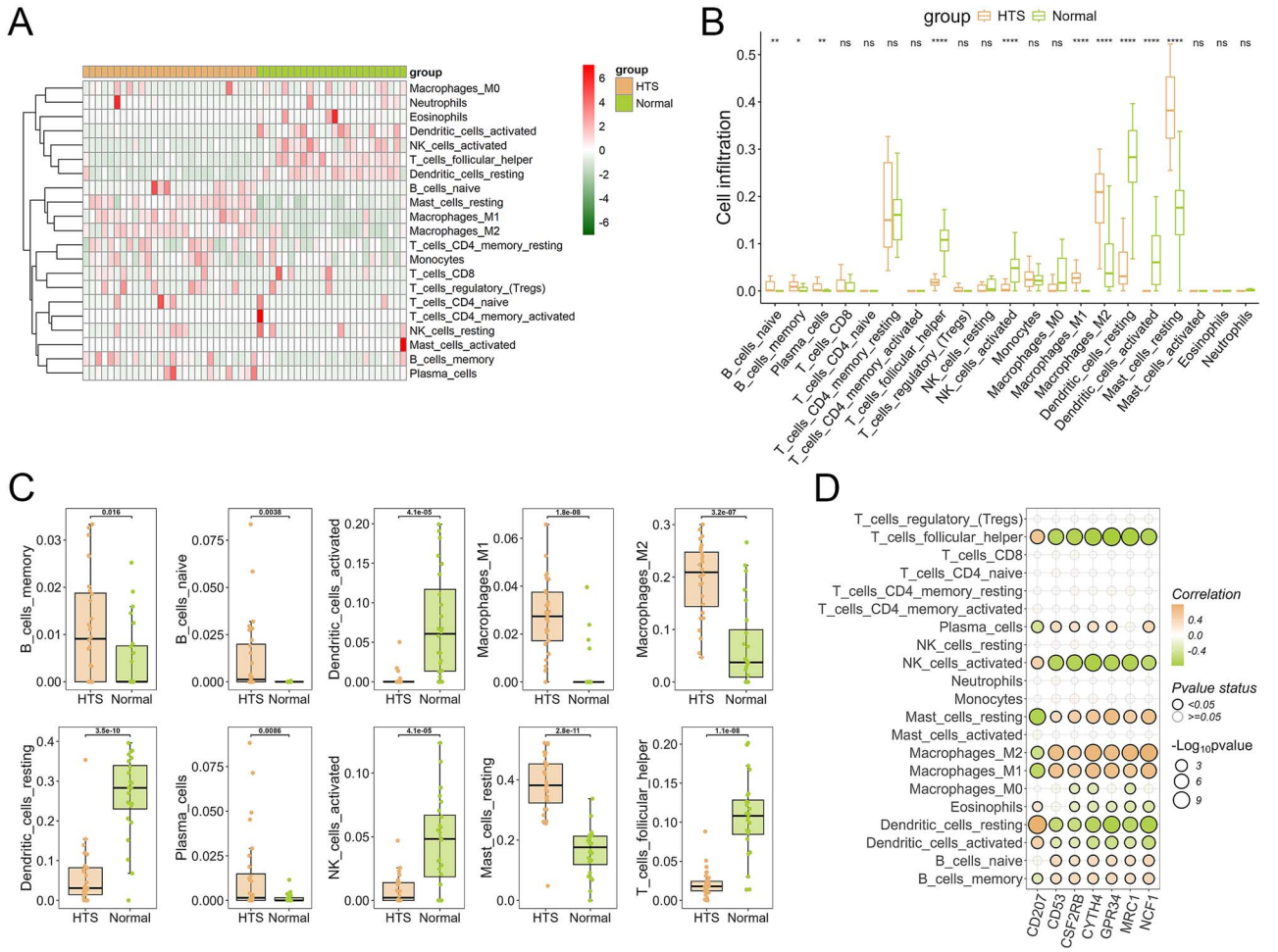


Figure 6. Immune Infiltration Landscape in HTS and Its Correlation With GPR34 and NCF1 Expression. (A) Overview of immune cell infiltration patterns in HTS samples. (B) and (C) Comparative analysis of immune cell subset infiltration between normal and HTS tissues. (D) Correlation matrix analysis demonstrating significant positive correlations between GPR34 and NCF1 expression and macrophage-related subsets (particularly M1 and M2 macrophages). Abbreviation: HTS = hypertrophic scar.

fication and fibrotic progression, whereas GTP-dependent small GTPases regulate macrophage migration, phagocytosis, and cytoskeletal remodeling, indirectly influencing immune cell retention and functional persistence within the wound microenvironment.[35,36] In scar formation research, attention has traditionally centered on canonical profibrotic and proinflammatory mediators such as TGF-β1, IL-6, and TNF-α, whereas systematic investigation of immunometabolic reprogramming remains relatively limited. At single-cell resolution, we observed a significant elevation in nucleotide metabolism pathway scores in HTS macrophages, accompanied by enrichment of differentially expressed genes in classical inflammatory pathways, including the NF-κB signaling pathway and the Toll-like receptor signaling pathway. These findings suggest that enhanced nucleotide metabolism provides essential biosynthetic substrates and energetic support for sustained inflammatory output, while inflammatory signaling reciprocally promotes activation of nucleotide biosynthetic pathways, forming a positive feedback loop. Considering the prolonged inflammatory phase and persistent fibroblast activation characteristic of HTS, we speculate that sustained upregulation of nucleotide metabolism constitutes a critical metabolic foundation for maintaining chronic macrophage activation and driving progressive scar hyperplasia.

On this basis, we sought to translate single-cell molecular signatures into a predictive tool with potential clinical applicability. By systematically evaluating 18 machine learning algorithms and their 112 combinations, we identified Enet + svmLinear as the optimal model. This model achieved consistently high AUC values across multiple independent cohorts, demonstrating robust performance and strong generalizability. These findings suggest that the molecular characteristics of HTS exhibit relatively stable expression patterns capable of distinguishing disease status across datasets. More importantly, SHAP analysis substantially enhanced model interpretability and enabled the identification of 7 key genes that contributed substantially to prediction performance, including CD207, CD53, CSF2RB, CYTH4, GPR34, MRC1, and NCF1. Among them, GPR34 and NCF1 showed the greatest contribution to model output, and their elevated expression levels were significantly associated with increased HTS risk. GPR34, a member of the GPCR family, has been reported to be highly

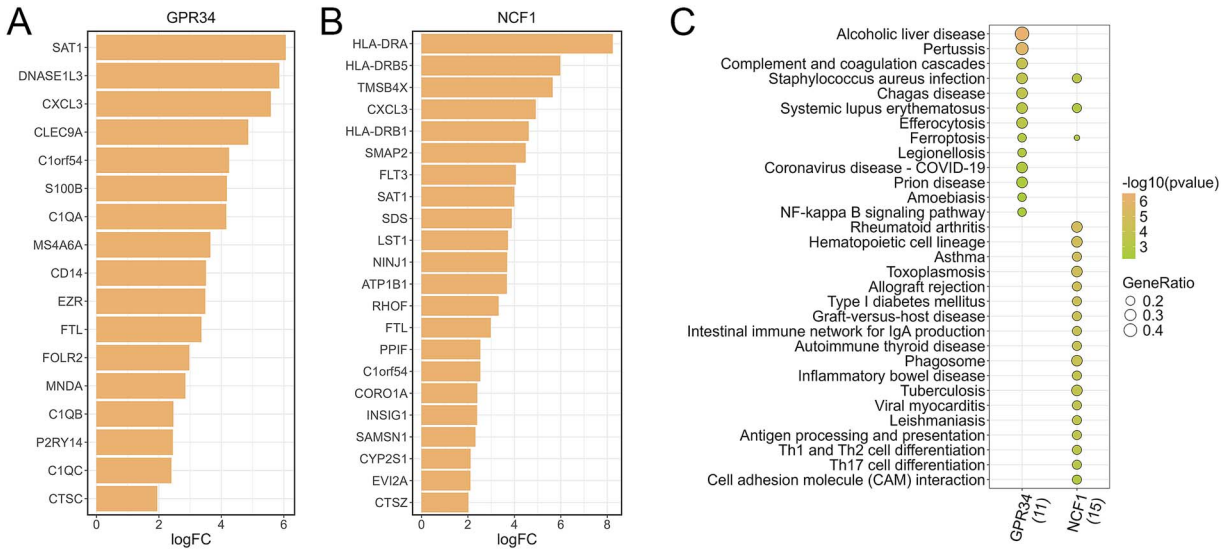


Figure 7. In Silico Virtual Knockout Analysis of GPR34 and NCF1 and Their Downstream Regulatory Effects in HTS. (A) Differential gene expression profile following virtual knockout of GPR34. (B) Transcriptomic alterations induced by virtual knockout of NCF1. (C) KEGG pathway enrichment analysis of differentially expressed genes after GPR34 and NCF1 virtual knockout. Abbreviation: HTS = hypertrophic scar; KEGG = Kyoto Encyclopedia of Genes and Genomes.

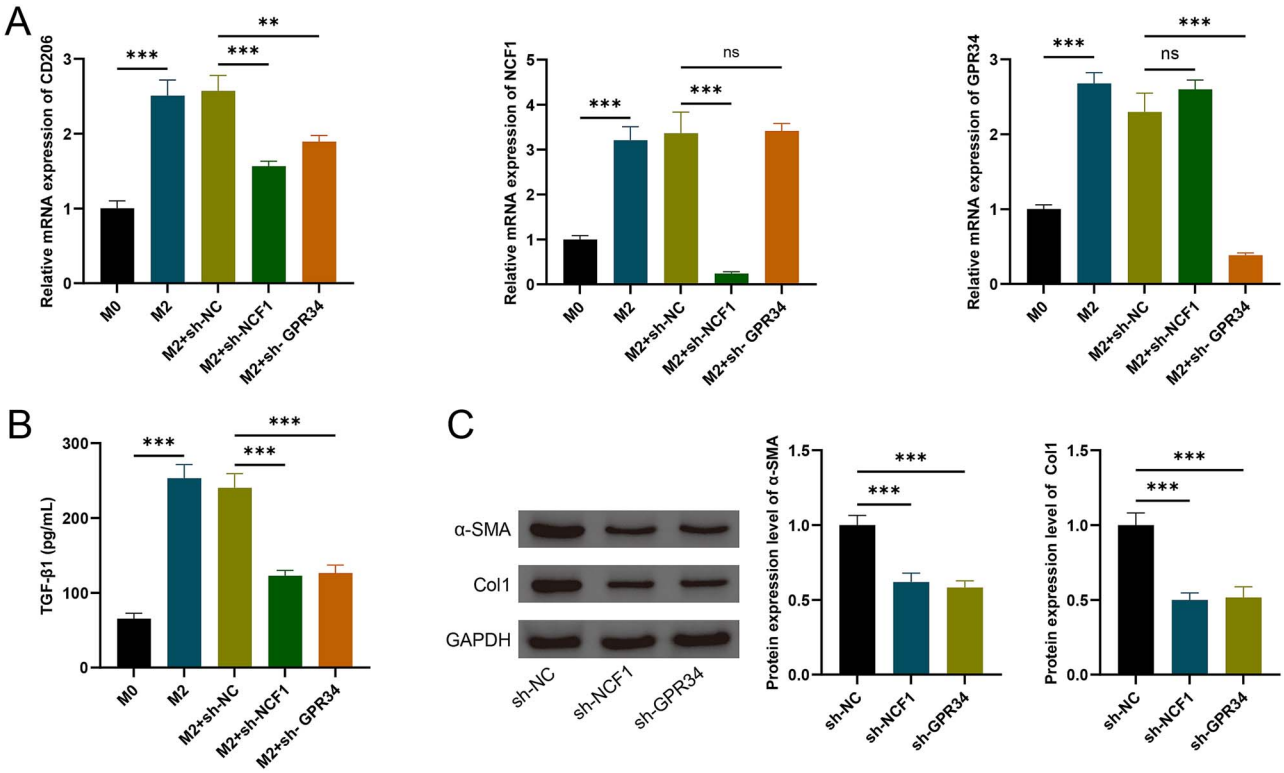


Figure 8. NCF1 and GPR34 Regulate M2 Macrophage Activation and Fibrotic Responses. (A) qRT-PCR analysis of CD206, NCF1, and GPR34 mRNA expression in THP-1-derived macrophages. (B) ELISA analysis of TGF-β1 secretion levels in the culture supernatants of THP-1-derived macrophages. (C) Western blotting analysis of α-SMA and collagen I (Col1) protein expression in human dermal fibroblasts after co-culture with THP-1-derived M2-sh-NC, M2-sh-NCF1, or M2-sh-GPR34 macrophages. All experiments were conducted at least 3 times, and data are presented as mean ± SD. ***$P < .001$; ns, not significant. Abbreviation: ELISA = enzyme-linked immunosorbent assay; qRT-PCR = quantitative real-time polymerase chain reaction; SMA = smooth muscle actin; TGF = transforming growth factor.

expressed in macrophages and microglia, where it participates in the regulation of tumor cell migration and proliferation.[37,38] NCF1 encodes a critical subunit of the NADPH oxidase complex and regulates reactive oxygen species (ROS) generation. Dysregulation of NCF1 function has been closely associated with persistent chronic inflammation, immune imbalance, and fibrotic diseases.[39–41] Previous studies have demonstrated that elevated ROS levels promote fibroblast activation, enhance collagen deposition, and potentiate TGF-β1 signaling pathway activity.[42,43] Taken together, GPR34-mediated immune cell recruitment and NCF1-driven oxidative stress amplification may contribute to scar microenvironment remodeling from 2 complementary dimensions: "inflammatory cell influx" and "inflammatory signal amplification." The concordance between predictive contribution and established biological function strengthens the credibility of our model and provides a mechanistic rationale for pathway-level interpretation. These findings suggest that GPR34 and NCF1 may occupy central nodes within the immune regulatory network of HTS, rather than serving merely as statistical biomarkers.

Further analyses demonstrated that samples with high GPR34 expression were significantly enriched in pathways related to immune cell migration and ECM interaction. GPR34 contributes to the survival and homeostatic maintenance of myeloid cells and can potentiate inflammatory signal amplification through activation of the downstream ERK and NF-κB signaling axes.[44] In fibrotic diseases, sustained recruitment of immune cells to sites of tissue injury is considered a critical event driving fibroblast activation and excessive ECM deposition.[45] Following in silico knockout of GPR34, we observed marked downregulation of complement-associated molecules, including C1QA, C1QB, C1QC, and CLEC9A, further supporting its functional involvement in innate immune recognition and phagocytic clearance. Beyond pathogen recognition, the complement system, particularly C1q-mediated macrophage polarization, has been implicated in tissue remodeling processes.[46,47] Collectively, these findings suggest that GPR34 may modulate immune homeostasis within the scar microenvironment through regulation of the complement–macrophage axis. Samples with high NCF1 expression were enriched in antigen processing and presentation pathways. Virtual knockout of NCF1 significantly altered the expression of MHC class II molecules, including HLA-DRA and HLA-DRB1, implying that NCF1 may enhance antigen-presenting capacity of dendritic cells or macrophages via ROS-dependent mechanisms. Previous studies have shown that NOX2-mediated ROS production regulates antigen processing efficiency and MHC class II expression,[48] thereby bridging innate and adaptive immune responses. This observation is consistent with the pathological coexistence of persistent inflammation and sustained immune activation in HTS.

At the signaling pathway level, both GPR34 and NCF1 were closely associated with the NF-κB signaling pathway, phagosome formation, and complement cascade activation. Nuclear factor-κB is widely recognized as a central inflammatory transcription factor in fibrogenesis, capable of promoting ECM remodeling through induction of TGF-β, IL-6, and related mediators.[49–51] Phagosome activity and complement activation cooperatively participate in the clearance of damage-associated molecular patterns and amplification of immune activation, thereby sustaining a chronic inflammatory microenvironment. In HTS, a scar subtype characterized by pronounced inflammatory activity, the coordinated activation of these pathways is pathophysiologically plausible. Importantly, when integrated with our earlier findings of enhanced nucleotide metabolism, these results further link immune activation with metabolic reprogramming. Activated immune cells typically exhibit increased purine and pyrimidine synthesis to support rapid proliferation and cytokine production.[52] Reactive oxygen species generation likewise depends on adequate NADPH supply, and nucleotide metabolism, together with the pentose phosphate pathway, plays a crucial role in maintaining intracellular NADPH homeostasis. Therefore, GPR34 and NCF1 likely function as pivotal molecular hubs connecting enhanced nucleotide metabolism with amplified immune-inflammatory signaling. Their regulatory roles along the integrated "metabolism–immunity–matrix remodeling" axis provide a theoretical foundation for subsequent mechanistic validation and the development of targeted therapeutic interventions.

Several limitations should be considered in this study. First, our findings were mainly based on transcriptomic data, and mRNA alterations do not always correspond to protein expression or functional activity. Although we performed in vitro validation of NCF1 and GPR34, further studies involving protein-level validation and in vivo models are required. Second, although bulk RNA sequencing provides larger sample sizes for biomarker identification, it cannot determine the specific cellular sources of transcriptional signals. We therefore integrated single-cell RNA sequencing data to provide cellular context; however, future studies using larger single-cell cohorts or spatial transcriptomics are needed for further validation. Third, the current analysis compared HTS with normal skin, which may capture both scar-related and HTS-specific changes. Prospective longitudinal studies comparing wounds that progress to HTS with those undergoing normal scar maturation will be necessary to identify early predictive biomarkers. Finally, the current machine learning model was developed from cross-sectional datasets and lacks temporal information. Future studies combining molecular signatures with clinical characteristics and longitudinal wound data may improve the clinical applicability of HTS prediction.

CONCLUSION

In summary, this study not only deepens the understanding of cellular composition and functional states in HTS at single-cell resolution but also establishes a molecular signature–based predictive model with translational potential. Moreover, we propose a conceptual framework centered on a continuous "metabolism–immunity–matrix remodeling" regulatory axis. This integrative perspective provides a systematic theoretical basis for elucidating the molecular mechanisms underlying HTS, identifying potential therapeutic targets, and advancing precision treatment strategies.

SUPPLEMENTARY MATERIAL

Supplementary material is available at *Journal of Burn Care & Research* online.

DATA AVAILABILITY

The data are available from the corresponding author upon reasonable request.

ETHICS APPROVAL AND CONSENT TO PARTICIPATE

In accordance with the Declaration of Helsinki, this research is based on open-source data, so the need for ethics approval was waived.

REFERENCES

1. Gao Y, Liu Y, Zheng D, et al. HDAC5-mediated Smad7 silencing through MEF2A is critical for fibroblast activation and hypertrophic scar formation. *Int J Biol Sci*. 2022;18:5724-5739. https://doi.org/10.7150/ijbs.76140
2. Zhang H, Zang C, Zhao W, et al. Exosome derived from mesenchymal stem cells alleviates hypertrophic scar by inhibiting the fibroblasts via TNFSF-13/HSPG2 signaling pathway. *Int J Nanomedicine*. 2023;18:7047-7063. https://doi.org/10.2147/IJN.S433510
3. He J, Fang B, Shan S, et al. Mechanical stretch promotes hypertrophic scar formation through mechanically activated cation channel Piezo1. *Cell Death Dis*. 2021;12:226. https://doi.org/10.1038/s41419-021-03481-6
4. Leszczynski R, da Silva CAP, Pinto ACPN, Kuczynski U, da Silva EMK. Laser therapy for treating hypertrophic and keloid scars. *Cochrane Database Syst Rev*. 2022;2022:Cd011642. https://doi.org/10.1002/14651858.CD011642.pub2
5. Wang J, Zhao M, Zhang H, et al. KLF4 alleviates hypertrophic scar fibrosis by directly activating BMP4 transcription. *Int J Biol Sci*. 2022;18:3324-3336. https://doi.org/10.7150/ijbs.71167
6. Zhang X, Sun J, Guo J, et al. Inhibition of adenosine/A2A receptor signaling suppresses dermal fibrosis by enhancing fatty acid oxidation. *Cell Commun Signal*. 2025;23:206. https://doi.org/10.1186/s12964-025-02210-2
7. Brizel HE, Scott RM. Palliative irradiation for bladder carcinoma. *Am J Roentgenol Radium Ther Nucl Med*. 1967;100:909-915.
8. Chandel NS. Nucleotide metabolism. *Cold Spring Harb Perspect Biol*. 2021;13:a040592. https://doi.org/10.1101/cshperspect.a040592
9. Madsen HB, Peeters MJW, Straten P, Desler C. Nucleotide metabolism in the regulation of tumor microenvironment and immune cell function. *Curr Opin Biotechnol*. 2023;84:103008. https://doi.org/10.1016/j.copbio.2023.103008
10. Ali ES, Ben-Sahra I. Regulation of nucleotide metabolism in cancers and immune disorders. *Trends Cell Biol*. 2023;33:950-966. https://doi.org/10.1016/j.tcb.2023.03.003
11. Suleiman H, Emerson A, Wilson PM, Mulligan KA, Ladner RD, LaBonte MJ. Harnessing nucleotide metabolism and immunity in cancer: a tumour microenvironment perspective. *FEBS J*. 2025;292:2155-2172. https://doi.org/10.1111/febs.17278
12. Barone N, Safran T, Vorstenbosch J, Davison PG, Cugno S, Murphy AM. Current advances in hypertrophic scar and keloid management. *Semin Plast Surg*. 2021;35:145-152. https://doi.org/10.1055/s-0041-1731461
13. Deng C, Zheng J, Wan W, et al. Suppression of cell proliferation and collagen production in cultured human hypertrophic scar fibroblasts by Sp1 decoy oligodeoxynucleotide. *Mol Med Rep*. 2013;7:785-790. https://doi.org/10.3892/mmr.2013.1278
14. Du J, Liu F, Liu X, et al. Lysosomal dysfunction and overload of nucleosides in thymidine phosphorylase deficiency of MNGIE. *J Transl Med*. 2024;22:449. https://doi.org/10.1186/s12967-024-05275-8
15. Vorstandlechner V, Copic D, Klas K, et al. The secretome of irradiated peripheral mononuclear cells attenuates hypertrophic skin scarring. *Pharmaceutics*. 2023;15:1065. https://doi.org/10.3390/pharmaceutics15041065
16. Ma L, Hua L, Yu W, Ke L, Li LY. TSG-6 inhibits hypertrophic scar fibroblast proliferation by regulating IRE1α/TRAF2/NF-κB signalling. *Int Wound J*. 2023;20:1008-1019. https://doi.org/10.1111/iwj.13950
17. Song B, Zhu Y, Zhao Y, et al. Machine learning and single-cell transcriptome profiling reveal regulation of fibroblast activation through THBS2/TGFβ1/P-Smad2/3 signalling pathway in hypertrophic scar. *Int Wound J*. 2024;21:e14481. https://doi.org/10.1111/iwj.14481
18. Zhang Q, Shi L, He H, et al. Down-regulating scar formation by microneedles directly via a mechanical communication pathway. *ACS Nano*. 2022;16:10163-10178. https://doi.org/10.1021/acsnano.1c11016
19. Li M, Wang P, Li J, et al. NRP1 transduces mechanical stress inhibition via LATS1/YAP in hypertrophic scars. *Cell Death Discov*. 2023;9:341. https://doi.org/10.1038/s41420-023-01635-3
20. Song B, Liu W, Zhu Y, et al. Deciphering the contributions of cuproptosis in the development of hypertrophic scar using single-cell analysis and machine learning techniques. *Front Immunol*. 2023;14:1207522. https://doi.org/10.3389/fimmu.2023.1207522
21. Tu L, Lin Z, Huang Q, Liu D. USP15 enhances the proliferation, migration, and collagen deposition of hypertrophic scar-derived fibroblasts by deubiquitinating TGF-βR1 in vitro. *Plast Reconstr Surg*. 2021;148:1040-1051. https://doi.org/10.1097/PRS.0000000000008488
22. Chen ZH, Yu B, Ye QF, Wang YF. Research advances on interleukin-6 in hypertrophic scar formation. *Zhonghua Shao Shang Yu Chuang Mian Xiu Fu Za Zhi*. 2022;38:874-877.
23. Zhou R, Wang C, Lv D, Sun Y, Liang Y. TNF-α inhibits fibrosis and migration of fibroblasts in hypertrophic scar by miR-141-3p. *Acta Biochim Biophys Sin Shanghai*. 2021;53:1106-1108. https://doi.org/10.1093/abbs/gmab086
24. Li T, Chen W, Zhang Q, Deng C. Human-specific gene CHRFAM7A mediates M2 macrophage polarization via the Notch pathway to ameliorate hypertrophic scar formation. *Biomed Pharmacother*. 2020;131:110611. https://doi.org/10.1016/j.biopha.2020.110611
25. Xia Z, Wang J, Yang S, et al. Emodin alleviates hypertrophic scar formation by suppressing macrophage polarization and inhibiting the Notch and TGF-β pathways in macrophages. *Braz J Med Biol Res*. 2021;54:e11184. https://doi.org/10.1590/1414-431x2021e11184
26. Feng Y, Sun ZL, Liu SY, et al. Direct and indirect roles of macrophages in hypertrophic scar formation. *Front Physiol*. 2019;10:1101. https://doi.org/10.3389/fphys.2019.01101
27. Shi M, Zhang L, Bi F, Ma X. Exosomes derived from M2 macrophages promote fibroblast autophagy to contribute to hypertrophic scar formation via CXCL2/CXCR7/mTOR pathway. *Hum Exp Toxicol*. 2024;43:9603271241303320. https://doi.org/10.1177/09603271241303320
28. Zhu Z, Chen B, Peng L, Gao S, Guo J, Zhu X. Blockade of LINC01605-enriched exosome generation in M2 macrophages impairs M2 macrophage-induced proliferation, migration, and invasion of human dermal fibroblasts. *Int J Immunopathol Pharmacol*. 2021;35:20587384211016724. https://doi.org/10.1177/20587384211016724
29. Lv X, Xiang C, Zheng Y, Lv XL, Zhou WX. Langerin(+) dendritic cells in cutaneous fibrosis: the TGF-β1 signaling axis. *Clin Cosmet Investig Dermatol*. 2025;18:2801-2828. https://doi.org/10.2147/CCID.S549199
30. Hong YK, Chang YH, Lin YC, Chen B, Guevara BEK, Hsu CK. Inflammation in wound healing and pathological scarring. *Adv Wound Care (New Rochelle)*. 2023;12:288-300. https://doi.org/10.1089/wound.2021.0161
31. Zhang X, Wu X, Li D. The communication from immune cells to the fibroblasts in keloids: implications for immunotherapy. *Int J Mol Sci*. 2023;24:15475. https://doi.org/10.3390/ijms242015475
32. John SV, Seim GL, Erazo-Flores BJ, et al. Classically activated macrophages undergo functionally significant nucleotide metabolism remodelling driven by nitric oxide. *Nat Metab*. 2025;7:1681-1702. https://doi.org/10.1038/s42255-025-01337-3
33. Bhatia D, Chung KP, Nakahira K, et al. Mitophagy-dependent macrophage reprogramming protects against kidney fibrosis. *JCI Insight*. 2019;4:e132826. https://doi.org/10.1172/jci.insight.132826
34. Wang J, Takemura N, Saitoh T. Macrophage response driven by extracellular ATP. *Biol Pharm Bull*. 2021;44:599-604. https://doi.org/10.1248/bpb.b20-00831
35. Roberts VS, Cowan PJ, Alexander SI, Robson SC, Dwyer KM. The role of adenosine receptors A2A and A2B signaling in renal fibrosis. *Kidney Int*. 2014;86:685-692. https://doi.org/10.1038/ki.2014.244
36. Travnickova J, Nhim S, Abdellaoui N, et al. Macrophage morphological plasticity and migration is Rac signalling and MMP9 dependant. *Sci Rep*. 2021;11:10123. https://doi.org/10.1038/s41598-021-88961-7
37. Schöneberg T, Meister J, Knierim AB, Schulz A. The G protein-coupled receptor GPR34—the past 20 years of a grownup. *Pharmacol Ther*. 2018;189:71-88. https://doi.org/10.1016/j.pharmthera.2018.04.008
38. Jin ZT, Li K, Li M, et al. G-protein coupled receptor 34 knockdown impairs the proliferation and migration of HGC-27 gastric cancer cells in vitro. *Chin Med J*. 2015;128:545-549. https://doi.org/10.4103/0366-6999.151114
39. Bakry O, Shoeib M, Soliman S, Kamal L. Neutrophil cytosolic factor-1 genotyping in acne vulgaris. *Skin Pharmacol Physiol*. 2021;34:51-56. https://doi.org/10.1159/000513053
40. Zhong J, Li Q, Holmdahl R. Natural loss-of-function mutations in Qa2 and NCF1 cause the spread of mannan-induced psoriasis. *J Invest Dermatol*. 2021;141:1765-1771.e4. https://doi.org/10.1016/j.jid.2021.01.006
41. Soleiman Ekhtiyari M, Yousefi M, Samadian F, et al. TNFRSF1A and NCF1 may act as hub genes in mastitis. *Vet Med Sci*. 2025;11:e70278. https://doi.org/10.1002/vms3.70278
42. Richter K, Kietzmann T. Reactive oxygen species and fibrosis: further evidence of a significant liaison. *Cell Tissue Res*. 2016;365:591-605. https://doi.org/10.1007/s00441-016-2445-3
43. Wu HH, Meng TT, Chen JM, et al. Asenapine maleate inhibits angiotensin II-induced proliferation and activation of cardiac fibroblasts via the ROS/TGFβ1/MAPK signaling pathway. *Biochem Biophys Res Commun*. 2021;553:172-179. https://doi.org/10.1016/j.bbrc.2021.03.042
44. Wu X, Cai J, Lin B, et al. GPR34-mediated sensing of lysophosphatidylserine released by apoptotic neutrophils activates type 3 innate

lymphoid cells to mediate tissue repair. *Immunity*. 2021;54:1123-1136.e8. https://doi.org/10.1016/j.immuni.2021.05.007

45. Odell ID, Steach H, Gauld SB, et al. Epiregulin is a dendritic cell-derived EGFR ligand that maintains skin and lung fibrosis. *Sci Immunol*. 2022;7:eabq6691. https://doi.org/10.1126/sciimmunol.abq6691
46. Hoeft K, Koch L, Ziegler S, et al. ADAMTS12 promotes fibrosis by restructuring extracellular matrix to enable activation of injury-responsive fibroblasts. *J Clin Invest*. 2024;134:e170246. https://doi.org/10.1172/JCI170246
47. Ogawa T, Shichino S, Ueha S, Ogawa S, Matsushima K. Complement protein C1q activates lung fibroblasts and exacerbates silica-induced pulmonary fibrosis in mice. *Biochem Biophys Res Commun*. 2022;603:88-93. https://doi.org/10.1016/j.bbrc.2022.02.090
48. Ligeon LA, Pena-Francesch M, Vanoaica LD, et al. Oxidation inhibits autophagy protein deconjugation from phagosomes to sustain MHC class II restricted antigen presentation. *Nat Commun*. 2021;12:1508. https://doi.org/10.1038/s41467-021-21829-6
49. Xue C, Mei CL. Polycystic kidney disease and renal fibrosis. *Adv Exp Med Biol*. 2019;1165:81-100. https://doi.org/10.1007/978-981-13-8871-2_5
50. Zhang L, Liu L, Bai M, et al. Hypoxia-induced HE4 in tubular epithelial cells promotes extracellular matrix accumulation and renal fibrosis via NF-κB. *FASEB J*. 2020;34:2554-2567. https://doi.org/10.1096/fj.201901950R
51. Micus LC, Trautschold-Krause FS, Jelit AL, Schön MP, Lorenz VN. NF-κB c-Rel modulates pre-fibrotic changes in human fibroblasts. *Arch Dermatol Res*. 2022;314:943-951. https://doi.org/10.1007/s00403-021-02310-2
52. Sugiura A, Andrejeva G, Voss K, et al. MTHFD2 is a metabolic checkpoint controlling effector and regulatory T cell fate and function. *Immunity*. 2022;55:65-81.e9. https://doi.org/10.1016/j.immuni.2021.10.011

© The Author(s) 2026. Published by Oxford University Press on behalf of the American Burn Association. This is an Open Access article distributed under the terms of the Creative Commons Attribution-NonCommercial License (https://creativecommons.org/licenses/by-nc/4.0/), which permits non-commercial re-use, distribution, and reproduction in any medium, provided the original work is properly cited. For commercial re-use, please contact reprints@oup.com for reprints and translation rights for reprints. All other permissions can be obtained through our RightsLink service via the Permissions link on the article page on our site—for further information please contact journals.permissions@oup.com.
https://doi.org/10.1093/jbcr/irag152
ORIGINAL ARTICLE